Improved Power Conversion Efficiency in Bulk Heterojunction Organic Solar Cells with Radial Electron Contacts

Jonathan E. Allen and Charles T. Black*

Center for Functional Nanomaterials, Brookhaven National Laboratory, Upton, New York 11973, United States

ABSTRACT We incorporate radial electrical contacts penetrating a blended organic semiconductor active layer to shorten the electron collection pathway in poly(3-hexylthiophene):[6,6]-phenyl-C_{61}-butyric acid methyl ester bulk heterojunction solar cells and simultaneously confine the blend material within nanometer-scale volumes. This architecture improves the active material performance by more than 50% compared to its performance in a bulk heterojunction with planar contacts, consistent with accelerated electron extraction. The radial contact solar cell achieves similar overall photovoltaic power conversion efficiency to control bulk heterojunction devices with planar contacts, despite containing less than half the volume of light-absorbing semiconductor material.

KEYWORDS: photovoltaic · organic · template · TiO_2 · atomic layer deposition · solar cell

Organic semiconductors can effectively convert solar radiation to electrical energy, and the most successful organic photovoltaic devices are based on a bulk heterojunction architecture.[1] Organic semiconductor solar cells offer significant benefits over their inorganic counterparts, including strong optical absorption, scalable processing, and the ability to fabricate devices on flexible substrates. However, the best reported devices offer power conversion efficiencies in the range 5−9%[2−6] due to limitations of the organic semiconductor materials. For example, a widely used organic solar cell active layer is a 1:1 blend of the polymer poly(3-hexylthiophene) (P3HT) and the small molecule [6,6]-phenyl-C_{61}-butyric acid methyl ester (PCBM), which can yield device power conversion efficiencies as high as ∼5%.[5] However, straightforward materials considerations suggest a maximum performance of these materials of at least 10%,[7] indicating that there are opportunities for optimizing even this well-studied structure.

The performance of bulk heterojunction solar cells can be improved by limiting the loss of photogenerated charge carriers during collection. Charge transport through organic materials is typically several orders of magnitude slower than in inorganic thin films, an especially unfortunate reality in bulk heterojunction devices because carriers are subject to interfacial recombination along the entire internal collection pathway. Significant research efforts have focused on realizing an ordered bulk heterojunction architecture aimed at optimizing the active layer morphology for effective charge collection.[8−10] Nanostructured electrodes penetrating the device active layer provide another approach for improving charge collection in randomly blended bulk heterojunction architectures.[11,12] Simulations of solar cells with photogenerated carrier collection in a radial direction (i.e., orthogonal to the incident light direction) suggest that this architecture can enhance the performance of poorly conducting active layer materials (Figure 1).[13] Here we demonstrate this concept in an organic bulk heterojunction solar cell using a fabrication scheme that allows us to independently evaluate the effects of nanoscale confinement and radial charge collection.

RESULTS AND DISCUSSION

In a blended P3HT:PCBM solar cell architecture, charge collection may be limited by the more poorly conducting of the two blend components when a discrepancy in their transport properties exists.[14,15] Measurements of the charge carrier mobility of each component material for our device structure show approximately equal electron and hole mobility in PCBM and P3HT, respectively. Our thin-film devices for measuring mobility sandwich the organic semiconductor between a bottom indium tin oxide (ITO) (200 nm)/TiO_2 (20 nm) electron-collecting contact and either a top aluminum contact (for PCBM devices) or a poly(3,4-ethylenedioxythiophene) poly(styrenesulfonate) (PEDOT:PSS) (40 nm)/Au

* Address correspondence to ctblack@bnl.gov.

Received for review June 29, 2011 and accepted September 12, 2011.

Published online September 12, 2011
10.1021/nn2031963

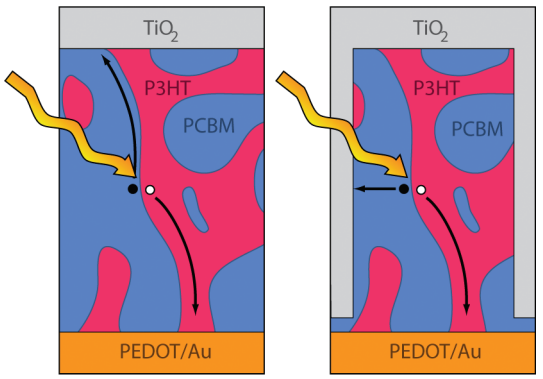

Figure 1. Schematic comparing charge collection in a bulk heterojunction solar cell with planar electrical contacts and a bulk hetereojunction with a radial electron contact.

(80 nm) contact (for P3HT devices) (Figure 2a).[14,16,17] In both devices, the forward bias current–voltage relation (*I*–*V*) displays a quadratic *V*-dependence characteristic of space-charge limited current (SCLC) (Figure 2b). Using the trap-free parallel plate model for SCLC,[18] we estimate an average PCBM electron mobility of $\sim(9 \pm 3) \times 10^{-4}$ $cm^2 V^{-1} s^{-1}$ and average P3HT hole mobility of $2 \times 10^{-3} \pm 4 \times 10^{-4}$ $cm^2 V^{-1} s^{-1}$, comparable values given the statistical uncertainty in our measurement (Figure 2c). Both these average values (based on measurements of four devices of each type) fall within the previously reported mobility ranges for P3HT and PCBM.[14,19]

Our device architecture simultaneously introduces radial charge-collecting contacts and also confines the P3HT:PCBM blend material to nanometer-scale volumes, which is known to increase P3HT hole mobility by disrupting perpendicular lamellar stacking.[17,20] Previously, we demonstrated that such confinement improves the performance of solar cell active layers formed on V_2O_5, which are limited by P3HT hole mobility.[17] Here, because we expect a similar P3HT hole mobility enhancement due to confinement, we anticipate the device performance to be limited by electron transport through the PCBM. By introducing radial TiO_2 electron-collecting pathways into the device architecture, electron transport distances within the PCBM are shortened. Previous studies of solar cells based on blended organic bulk heterojunctions and TiO_2 nanotubes have shown that this structure can produce promising power conversion efficiencies of 4.1%, with device photocurrents as high as 12.4 mA/cm^2.[21,22] Our device fabrication scheme allows us to separate the beneficial effects of nanometer-scale confinement of the blended organic active layer and radial charge collection. We confine the P3HT:PCBM blend within the hexagonally arranged pores of an anodized aluminum oxide template (two weight percent chlorobenzene solution spin coated in ambient air), positioned between a bottom transparent ITO (200 nm)/TiO_2 (20 nm) electron-collecting contact

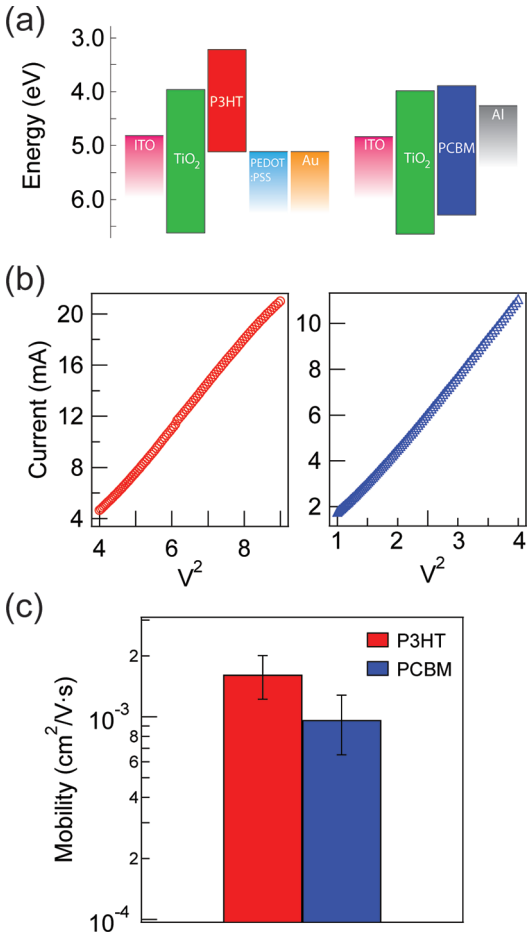

Figure 2. SCLC mobility measurements of P3HT and PCBM. (a) Energy band diagrams for devices fabricated to measure SCLC mobility in single-component P3HT and PCBM. (b) *I*–V^2 plots showing quadratic dependence of current on voltage in P3HT (red circles) and PCBM (blue triangles). (c) Hole (electron) mobilities for P3HT (PCBM) on TiO_2-coated substrates. Values are averages across four devices for each material with standard deviation indicated by the error bars.

and a top PEDOT:PSS (40 nm)/Au (80 nm) hole-collecting contact (Figure 3). The confining aluminum oxide template has a mean pore diameter of 70 nm and nearest-neighbor separation of 110 nm, so that a completely filled template contains 38% as much P3HT:PCBM compared to a planar blend film of the same thickness. Conformally lining the confining aluminum oxide with the radial electron contact material (11 nm TiO_2 (anatase), deposited by atomic layer deposition) prior to template infiltration with the P3HT:PCBM blend allows a direct comparison between confined blend devices and those having an additional radial electron contact. The radial contact reduces the average pore diameter by approximately 20 nm, potentially having consequences on the confined organic material structure and therefore electronic mobility and light absorption. While our experiments cannot distinguish these changes from the effect of the radial electron contact, previous studies suggest that such a reduction

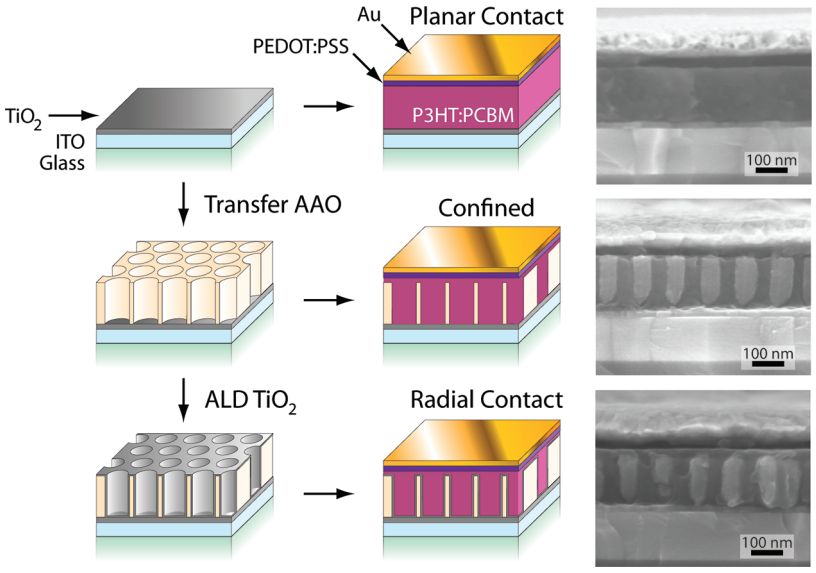

Figure 3. Fabrication process for inverted, confined bulk heterojunction solar cells. Top row: Control devices with planar contacts fabricated on TiO_2-coated ITO/glass substrates. Middle row: Confined devices fabricated by infiltrating the P3HT:PCBM blend into nanoporous aluminum oxide. Bottom row: Radial contact devices fabricated by infiltrating the blend into TiO_2-coated nanoporous aluminum oxide.

in confining pore diameter has a relatively small impact on these device parameters.[17,20]

Introducing radial TiO_2 electron-collecting contacts into the confined P3HT:PCBM blend active layer (160 nm thick) increases the device power conversion efficiency by 70% on average, compared to confined devices without radial contacts, from 1.1% ± 0.1% to 1.9% ± 0.2%. Both confined and radial contact devices achieve these efficiency values despite utilizing less than 50% of the active material compared to control bulk heterojunction devices utilizing planar contacts (due to space wasted by the confining Al_2O_3 template). We measured all devices in ambient conditions under 100 mW/cm^2 simulated AM1.5G illumination, calibrated using a certified KG5 filtered silicon reference cell.[23] At least four devices of each type were measured. Illuminated $J-V$ characteristics of the confined and radial contact devices (Figure 4a) have short-circuit photocurrent densities, J_{SC} = 3.2 ± 0.1 and 6.2 ± 0.4 mA/cm^2 for the confined and radial contact devices, respectively, and approximately the same open circuit voltage of 0.57−0.59 V. Despite containing less than half the amount of semiconductor blend compared to a sample of the same thickness with planar contacts, both confined and radial contact devices display significantly enhanced forward biased conductivity (Figure 4a inset), most likely due to improved hole mobility in the confined P3HT.[17,20] As well, the radial collection devices have a very short channel near the template top, where only a thin residual P3HT:PCBM blend layer separates the TiO_2 and PEDOT:PSS contact layers.

Optical transmission measurements show that both the confined and radial contact P3HT:PCBM active layer samples absorb significantly less incident light compared to a planar blend film of the same thickness (Figure 4b). We converted optical transmission spectra to absorption by assuming that all untransmitted light was absorbed (*i.e.*, neglecting reflection and scattering), and thus our measurements represent an upper bound on absorption. The integrated absorption over the measured range (350 to 900 nm) in the planar blend film was 2.2 times larger than that of a P3HT:PCBM film confined in a template with TiO_2 radial contact, in reasonable agreement with the difference in volume of organic material of the two samples. Accounting for the porosity of the TiO_2-coated Al_2O_3 template as well as a 20−30 nm film of excess blend material on top, we can estimate that radial contact devices contain ~40% as much active material as a control device with planar contacts (giving an expected absorption difference of 2.5 times). We can therefore reasonably rule out any significant light-scattering contribution that would increase the active layer absorption in the confined and radial contact devices. Devices with radial contacts output 70% as much photocurrent compared to the control, despite absorbing 45% as much light, consistent with a 55% improvement in total internal quantum efficiency integrated across the absorption spectrum.

Normalizing the measured device current density by the relative light absorption of the different active layers gives an effective current density that more clearly highlights the enhanced charge collection in devices having radial electron contacts (Figure 4c) and provides a comparison of the P3HT:PCBM material performance in the three different device architectures: a bulk heterojunction with planar contacts,

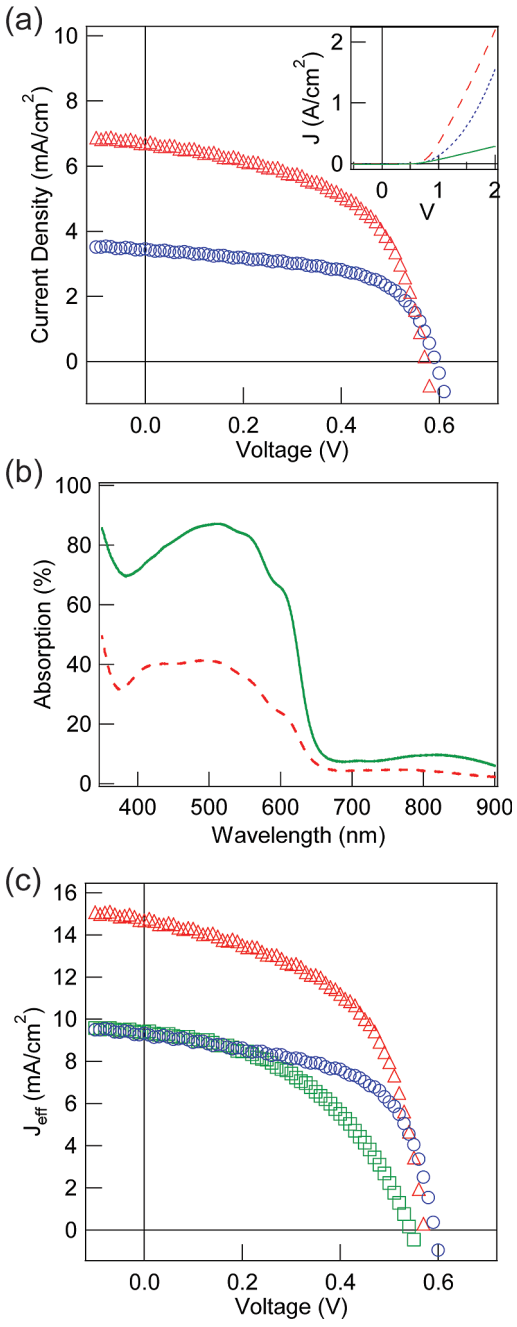

Figure 4. Photovoltaic device performance. (a) Current density *versus* voltage for confined (blue circles) and radial contact (red triangles) devices under illumination. Active layer thickness for both devices is ~160 nm. Inset: Dark *J*–*V* in forward bias for planar contact (green, solid), confined (blue, dotted), and radial contact (red, dashed) devices. (b) Light absorption *versus* wavelength for planar contact (green, solid) and radial contact (red, dashed) films, 220 nm thick. (c) Effective current density *versus* voltage data under illumination after normalizing for light absorption for planar (green squares), confined (blue circles), and radial contact (red triangles) devices.

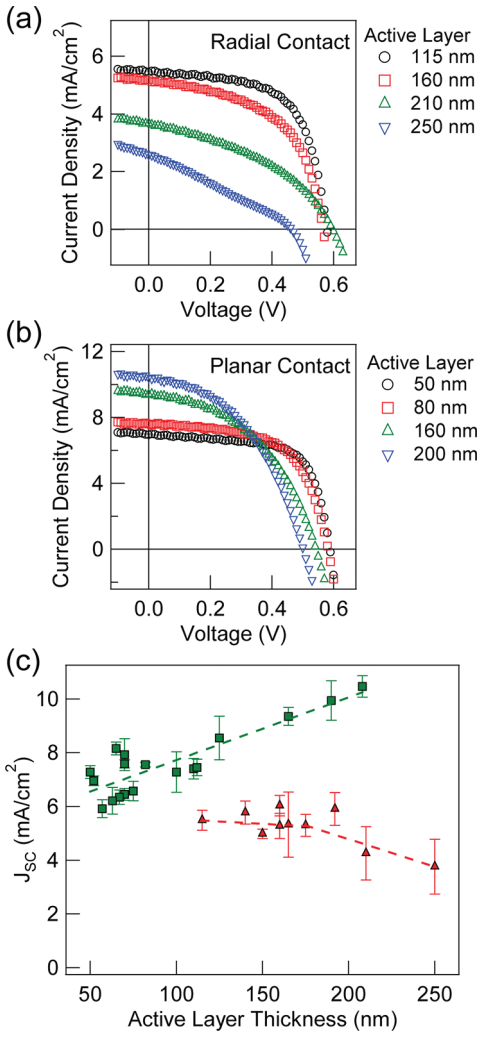

Figure 5. Solar cell performance *versus* active layer thickness for (a) radial contact and (b) planar contact devices. (c) J_{SC} *versus* active layer thickness for planar contact (green squares) and radial contact (red triangles) devices. Each data point represents an average from 3 to 5 devices with standard deviation indicated by error bars.

a confined bulk heterojunction, and a confined bulk heterojunction with radial electron contacts. The blend material in confined devices performs slightly better than when it is placed in a control device with planar contacts; however, we do not measure any improvement in the effective short-circuit current density. Because we expect an improved P3HT hole mobility in these devices,[17,20] this observation further supports that hole mobility does not limit charge collection in bulk heterojunctions fabricated on TiO_2. The small material performance enhancement in the confined device instead comes from an improved fill factor likely arising from the reduced series resistance. However, the same P3HT:PCBM blend material in a confined device with radial contacts shows a 95% improvement in power conversion efficiency compared to the material in a bulk heterojunction with planar contacts, due to improved fill factor (from 0.45 to 0.55) and a 55% increase in the effective short-circuit current density (from 9.4 to 14.6 mA/cm^2). A radial contact device of this type without any wasted template area would perform with power conversion efficiency of ~4.5%, generating ~80% of the maximum

possible photocurrent for a 1.85 eV band-gap light absorber.[7] These values are in good agreement with the performance of previous P3HT:PCBM devices incorporating TiO_2 nanotubes into the architecture.[21]

Increasing the confined P3HT:PCBM thickness of devices with radial electron contacts from 115 to 180 nm results in little change in photovoltaic performance, despite increased light absorption by the thicker active layer (Figure 5a,b). Beyond 180 nm, we measure a significant decrease in power conversion efficiency (due to reduced J_{SC} and fill factor) (Figure 5a, c). We have confirmed complete template filling by the organic material using cross sectional scanning electron microscopy of the measured devices, thus ruling out effects due to nonuniform organic material thicknesses. The observed behavior is consistent with internal electric field screening by the radial electrical contact geometry, leading to reduced photocurrent output from blend material located deeper within the template pores. Further increases in active layer thickness reduce fill factor and V_{OC} because of recombination within the active material and also at the TiO_2/P3HT interface. In contrast, control P3HT:PCBM blend devices with planar contacts show a steadily increasing J_{SC} with increasing active layer thickness from 50 to 200 nm, accompanied by steady decreases in fill factor and V_{OC} because of increased series resistance and recombination (Figure 5b,c).[24]

We have improved the photovoltaic performance of a blended P3HT:PCBM material by confining it to nanometer-scale volumes and introducing radial electron-collecting contacts into the device active layer. Our device fabrication scheme allows us to separate the beneficial effects of confining the blend and incorporating radial contacts into the bulk heterojunction architecture. Confining the active material significantly improves its conductivity, consistent with improved P3HT mobility and resulting in improved device fill factor. Introducing a radial TiO_2 electron contact increases the device total internal quantum efficiency more than 50% by improving electron collection efficiency.

METHODS

Fabrication of Nanoporous Aluminum Oxide Templates. A two-step anodization processes using high-purity (99.999%) aluminum sheets (ESPI Metals) yielded highly ordered nanoporous aluminum oxide films. All anodization was performed at 40 V at room temperature in 0.4 M oxalic acid. After anodizing for one hour, the resulting oxide layer (~12 μm thick) was stripped using a 0.4 M phosphoric acid/0.2 M chromic acid solution heated at 85 °C for 45 min. The substrates were anodized a second time for 42–90 s, depending on the desired template thickness (100–300 nm). All templates were then etched in 5 wt % phosphoric acid for 30 min at room temperature in order to widen the pore diameters to ~50–60 nm.

Nanoporous Aluminum Oxide Pattern Transfer Procedure. The completed, hexagonally ordered aluminum oxide templates were transferred to device substrates using the following procedure. A protective PMMA layer (Microchem 950PMMA C4) was spin-cast on top of the template at 1000 rpm and subsequently baked on a hot plate at 180 °C for 90 s. The aluminum substrate was removed using a solution of 20 mL of H_2O, 20 mL of HCl, and 1 g of $CuCl_2$, leaving only the aluminum oxide template and the protective PMMA layer. After rinsing in water, the structure was then etched in 5 wt % phosphoric acid for 2 h to expose the pore bottoms. During this step the PMMA layer protected the pore interiors until the pore bottoms were opened. There is additional pore widening after the etchant enters the template and begins to etch the pore interiors. This typically results in ~10 nm of additional pore widening. Finally, the templates are transferred to an acetone bath, where the PMMA is dissolved, leaving only the template behind. The templates are physically transferred to the desired device substrate and blown dry using nitrogen.

Solar Cell Fabrication: Planar Contact Devices. Commercial ITO-coated glass substrates were first coated with 20 nm of TiO_2 by atomic layer deposition followed by spin coating of a 1:1 blend of P3HT:PCBM (2% in chlorobenzene) in ambient air. Spin speed was varied between 400 and 1300 rpm to vary the film thickness. The top contact consisted of a 40 nm layer of PEDOT:PSS (33% in IPA to aid wetting on the organic active layer, spin-coated at 3000 rpm for 45 s) and an 80 nm Au film deposited by thermal evaporation. *Confined Devices:* Devices with confined active layers were fabricated in the same way except that a nanoporous aluminum oxide template was first transferred to the TiO_2-coated substrate before spin coating the active material using the procedure listed above. Spin speed was kept constant at 1300 rpm regardless of template height, allowing the blend to completely fill the template while leaving minimal excess material on the top surface. *Radial Contact Devices:* Inverted devices with radial contacts were made by transferring the aluminum oxide templates to substrates with 9 nm thick layers of TiO_2 and subsequently depositing an additional 11 nm of TiO_2 by ALD before filling the template with the active material. We note that the confined devices and radial contact devices were fabricated in parallel. Templates for both types of devices were fabricated at the same time, and the TiO_2 films were deposited in the same ALD runs. Therefore the 20 nm TiO_2 film in the uncoated confined device was actually deposited in two ALD runs (one 9 nm deposition and one 11 nm deposition).

Acknowledgment. The authors acknowledge C.-Y. Nam (CFN) for helpful discussions regarding device performance. Research was carried out at the Center for Functional Nanomaterials, Brookhaven National Laboratory, which is supported by the U.S. Department of Energy, Office of Basic Energy Sciences, under Contract No. DE-AC02-98CH10886. Additional support was provided by Brookhaven Laboratory Research and Development Award 08-043.

REFERENCES AND NOTES

1. Yu, G.; Gao, J.; Hummelen, J. C.; Wudl, F.; Heeger, A. J. Polymer Photovoltaic Cells: Enhanced Efficiencies via a Network of Internal Donor-Acceptor Heterojunctions. *Science* **1995**, *270*, 1789–1791.
2. Liang, Y.; Feng, D.; Wu, Y.; Tsai, S.-T.; Li, G.; Ray, C.; Yu, L. Highly Efficient Solar Cell Polymers Developed via Fine-Tuning of Structural and Electronic Properties. *J. Am. Chem. Soc.* **2009**, *131*, 7792–7799.
3. Liang, Y.; Xu, Z.; Xia, J.; Tsai, S.-T.; Wu, Y.; Li, G.; Ray, C.; Yu, L. For the Bright Future - Bulk Heterojunction Polymer Solar Cells with Power Conversion Efficiency of 7.4%. *Adv. Mater.* **2010**, *22*, E135–E138.

4. Park, S. H.; Roy, A.; Beaupre, S.; Cho, S.; Coates, N.; Moon, J. S.; Moses, D.; Leclerc, M.; Lee, K.; Heeger, A. J. Bulk Heterojunction Solar Cells with Internal Quantum Efficiency Approaching 100%. *Nat. Photonics* **2009**, *3*, 297–302.
5. Ma, W.; Yang, C.; Gong, X.; Lee, K.; Heeger, A. J. Thermally Stable, Efficient Polymer Solar Cells with Nanoscale Control of the Interpenetrating Network Morphology. *Adv. Funct. Mater.* **2005**, *15*, 1617–1622.
6. Service, R. F. Outlook Brightens for Plastic Solar Cells. *Science* **2011**, *332*, 293.
7. Dennler, G.; Scharber, M. C.; Brabec, C. J. Polymer-Fullerene Bulk-Heterojunction Solar Cells. *Adv. Mater.* **2009**, *21*, 1323–1338.
8. He, X.; Gao, F.; Tu, G.; Hasko, D. G.; Hüttner, S.; Greenham, N. C.; Steiner, U.; Friend, R. H.; Huck, W. T. S. Formation of Well-Ordered Heterojunctions in Polymer:PCBM Photovoltaic Devices. *Adv. Funct. Mater.* **2011**, *21*, 139–146.
9. Kim, J. S.; Park, Y.; Lee, D. Y.; Lee, J. H.; Park, J. H.; Kim, J. K.; Cho, K. Poly(3-hexylthiophene) Nanorods with Aligned Chain Orientation for Organic Photovoltaics. *Adv. Funct. Mater.* **2010**, *20*, 540–545.
10. Wang, H.-S.; Chen, S.-Y.; Su, M.-H.; Wang, Y.-L.; Wei, K.-H. Inverted Heterojunction Solar Cells Incorporating Fullerene/Polythiophene Composite Core/Shell Nanorod Arrays. *Nanotechnology* **2010**, *21*, 145203.
11. Takanezawa, K.; Hirota, K.; Wei, Q.-S.; Tajima, K.; Hashimoto, K. Efficient Charge Collection with ZnO Nanorod Array in Hybrid Photovoltaic Devices. *J. Phys. Chem. C* **2007**, *111*, 7218–7223.
12. Baek, W.-H.; Seo, I.; Yoon, T.-S.; Lee, H. H.; Yun, C. M.; Kim, Y.-S. Hybrid Inverted Bulk Heterojunction Solar Cells with Nanoimprinted TiO_2 Nanopores. *Sol. Energy Mater. Sol. Cells* **2009**, *93*, 1587–1591.
13. Kayes, B. M.; Atwater, H. A.; Lewis, N. S. Comparison of the Device Physics Principles of Planar and Radial p-n Junction Nanorod Solar Cells. *J. Appl. Phys.* **2005**, *97*, 114302–114311.
14. Mihailetchi, V. D.; Xie, H. X.; de Boer, B.; Koster, L. J. A.; Blom, P. W. M. Charge Transport and Photocurrent Generation in Poly(3-hexylthiophene): Methanofullerene Bulk-Heterojunction Solar Cells. *Adv. Funct. Mater.* **2006**, *16*, 699–708.
15. Yang, F.; Forrest, S. R. Photocurrent Generation in Nanostructured Organic Solar Cells. *ACS Nano* **2008**, *2*, 1022–1032.
16. Nam, C.-Y.; Su, D.; Black, C. T. High-Performance Air-Processed Polymer-Fullerene Bulk Heterojunction Solar Cells. *Adv. Funct. Mater.* **2009**, *19*, 3552–3559.
17. Allen, J. E.; Yager, K. G.; Hlaing, H.; Nam, C.-Y.; Ocko, B. M.; Black, C. T. Enhanced Charge Collection in Confined Bulk Heterojunction Organic Solar Cells. *Appl. Phys. Lett.*, **2011**, *99*, in press.
18. Lampert, M. A.; Mark, P. *Current Injection in Solids*; Academic Press: New York, 1970.
19. Sirringhaus, H.; Brown, P. J.; Friend, R. H.; Nielsen, M. M.; Bechgaard, K.; Langveld-Voss, B. M. W.; Spiering, A. J. H.; Janssen, R. A. J.; Meijer, E. W.; Herwig, P.; *et al*. Two-Dimensional Charge Transport in Self-Organized, High-Mobility Conjugated Polymers. *Nature* **1999**, *401*, 685–688.
20. Coakley, K. M.; Srinivasan, B. S.; Ziebarth, J. M.; Goh, C.; Liu, Y.; McGehee, M. D. Enhanced Hole Mobility in Regioregular Polythiophene Infiltrated in Straight Nanopores. *Adv. Funct. Mater.* **2005**, *15*, 1927–1932.
21. Mor, G. K.; Shankar, K.; Paulose, M.; Varghese, O. K.; Grimes, C. A. High Efficiency Double Heterojunction Polymer Photovoltaic Cells Using Highly Ordered TiO_2 Nanotube Arrays. *Appl. Phys. Lett.* **2007**, *91*, 152111.
22. Yu, B.-Y.; Tsai, A.; Tsai, S.-P.; Wong, K.-T.; Yang, Y.; Chu, C.-W.; Shyue, J.-J. Efficient Inverted Solar Cells Using TiO_2 Nanotube Arrays. *Nanotechnology* **2008**, *19*, 255202.
23. Shrotriya, V.; Li, G.; Yao, Y.; Moriarty, T.; Emery, K.; Yang, Y. Accurate Measurement and Characterization of Organic Solar Cells. *Adv. Funct. Mater.* **2006**, *16*, 2016–2023.
24. Lenes, M.; Koster, L. J. A.; Mihailetchi, V. D.; Blom, P. W. M. Thickness Dependence of the Efficiency of Polymer:Fullerene Bulk Heterojunction Solar Cells. *Appl. Phys. Lett.* **2006**, *88*, 243502.